New highlights on phytolith structure and occluded carbon location: 3D X-ray microscopy and NanoSIMS results

A. Alexandre[1], I. Basile-Doelsch[1], T. Delhaye[2], D. Borschneck[1], J.C. Mazur[1], P. Reyerson[3], G. M. Santos[4]

n phytolith structure and occluded carbon location: 3D X-ray microscopy and NanoSIMS results

[1] Centre Européen de Recherche et d'Enseignement des Géosciences de l'Environnement (UMR 7330), CNRS, Aix-Marseille Université, Europôle méditerranéen de l'Arbois BP 80, 13545 Aix en Provence cedex 04, France

[2] Plateforme NanoSIMS, OSUR, Université de Rennes 1, Campus de Beaulieu, 35042 Rennes Cedex, France

[3] Department of Geography, University of Wisconsin-Madison, 550 North Park Street, Madison, WI 53706, USA

[4] Earth System Science, University of California, Irvine, B321 Croul Hall, Irvine, CA 9269, 3100, USA

Correspondence e-mail : alexandre@cerege.fr

Abstract

Phytoliths contain occluded organic compounds called phytC. Recently, phytC content, nature, origin, paleoenvironmental meaning and impact in the global C cycle has been the subject of increasing debate. Inconsistencies were fed by the scarcity of in-situ characterization of phytC in phytoliths. Here we reconstructed at high spatial resolution the 3-dimensional structure of harvested grass short cell (GSC) phytoliths using 3D X-ray microscopy. While this technic has been widely used for 3D reconstruction of biological systems it has never been applied in high resolution mode to silica particles. Simultaneously, we investigated the location of phytC using Nano-scale Secondary Ion Mass Spectrometry (NanoSIMS). Our data evidenced that the silica structure contains micrometric internal cavities. These internal cavities were sometimes observed isolated from the outside. Their opening may be an original feature or may result from a beginning of dissolution of silica during the chemical extraction procedure, mimicking the progressive dissolution process that can happen in natural environments. The phytC that may originally occupy the cavities is thus susceptible to rapid oxidation. It was not detected by the nanoSIMS technique. To the contrary another pool of phytC, continuously distributed in and protected by the silica structure was evidenced. Its N/C ratio (0.27) is in agreement with the presence of amino acids. These findings constitute a basis to further characterize the origin, occlusion process, nature and accessibility of phytC, as a prerequisite for assessing its significance in the global C cycle.

1. Introduction

When absorbing nutrients in the soil, plants roots also uptake a significant amount of silicon (Si). The Si fluxes recycled by plants are substantial: as an example Si take up by tropical forests or grasslands can reach twice to 10 times Si fluxes generated from the dissolution of soil silicates that are exported to stream waters (e.g. Blecker et al., 2006; Struyf and Conley, 2009; Cornelis, 2011; Alexandre et al., 2011). Inside the plant, Si is transported in the sap and deposited inside the cells, in the cell walls and in extracellular spaces of stems and leaves as micrometric hydrous amorphous silica particles called phytoliths. Upon plant decay, part of the phytolith production can be incorporated into soils or sediments and preserved for up to millions of years (Alexandre et al., 2011; Miller et al., 2012; Strömberg et al., 2013). Those fossil phytolith assemblages can be used for reconstructing past vegetation and climate conditions via their morphological and geochemical signatures (Piperno, 2006; Alexandre et al., 2012). Phytoliths occlude small amounts of organic compounds, first evidenced by the production of

carbon (C) and nitrogen (N) during dry ashing (Jones and Beavers, 1963). Later on, scanning transmission electron microscopy (STEM) and Energy Dispersive X-Ray (EDX) analyses of phytoliths in the plant tissues confirmed that the occluded organic compounds contained C, N and phosphorus (P) (Laue et al., 2007). By extension, these occluded compounds are here called phytC. PhytC, which is assumed to be protected from natural oxidation by the siliceous structure, has been the subject of increasing attention and debate.

Based on the assumption that phytC originated from the photosynthesis of atmospheric CO_2 in the host plant, several studies used phytC ^{14}C and $\delta^{13}C$ signatures, respectively as a dating tool (Piperno and Becker, 1996; Piperno and Stothert, 2003; McMichael et al., 2012) and a paleoenvironmental proxy (Kelly, 1991; Smith and White, 2004; Carter, 2009; Webb and Longstaffe, 2010; McInerney et al., 2011). However, very recently, ^{14}C-AMS measurements of phytC samples from modern grasses yielded ages of several thousand years, which suggested that phytoliths may incorporate a substantial amount of old carbon, potentially from the soil (Santos et al., 2010; Santos et al., 2012). Amino acids from soils have been shown to be taken up by plants, and transported in small proportion to roots, stems and shoots (Paungfoo-Lonhienne et al., 2008; Whiteside et al., 2009 ; Gao et al., 2010; Warren, 2012; Whiteside et al., 2012). Thus it is not inconsistent to assume that C and N derived from these soil amino acids have been trapped in phytoliths. Although the hypothesis still needs to be verified, it raised the question of the molecular nature of phytC. Several techniques such as High-performance liquid chromatography (HPLC), amino acid analyser, gas chromatography mass spectrometry (GC-MS), protein staining, micro-Raman analysis or X-Ray photoelectron spectroscopy (XPS) were used to characterize phytC and led to contradictory results, especially regarding the presence or not of amino acids (Harrison, 1996; Pironon et al., 2001; Smith and Anderson, 2001; Elbaum et al., 2009; Watling et al., 2011). The problem is that these methods were applied on phytolith concentrates that were not proven to be completely devoid of extraneous organic remains. Chemical extractions leading to high purity phytolith concentrates are indeed difficult to implement. Although the absence of organic particles can be checked by Scanning Electron Microscopy (SEM) coupled with EDX (Corbineau et al., 2013), the presence of extraneous organic remains on the phytolith surface cannot be accurately detected.

Differences in the efficiency of phytolith extraction protocols may also explain the inconsistencies in phytC quantification. Accurately quantifying the phytC is important for the assessment of its significance in the terrestrial C cycle. Multiple studies recently claimed that phytC may play a role in atmospheric CO_2 sequestration and climate change mitigation (Parr

and Sullivan, 2005; Parr et al., 2010; Song et al., 2013 ; Huang et al., 2014; Li et al., 2014; Song et al., 2014; Zuo et al., 2014), although the fluxes of phytC from vegetation to soils and the residence time of phytC in soils are still largely unknown. PhytC content as high as 20% dry weight was obtained when using a phytolith extraction method based on microwave digestion (Parr and Sullivan, 2014). This value was more than 20 to 200 times higher than the values obtained using a chemical method verified to be 100% efficient for removing extraneous organic particles (from 0.1 to 1% dry weight; Smith and White, 2001). The difference was somewhat justified by partial dissolution of phytC when using aggressive protocols. The assumption that phytC may be located at different sites in the silica structure, with different accessibility to oxidation, was put forward (Parr and Sullivan, 2014). This assumption supplemented a previous one, widely found in the literature, that micrometric opaque areas observed by Natural Light (NL) microscopy on some phytoliths, were holes containing the phytC (Prychid et al., 2003; Piperno, 2006; Carter et al., 2009; Song et al., 2012; Parr and Sullivan, 2014). No measurements were however performed to support any of these hypotheses.

Finally, the debates on content, location, nature, origin and paleoenvironmental meaning of phytC were fed by the scarcity of in-situ characterization of phytC in phytoliths, despite few seminal works (Harrison, 1996; Laue et al., 2007). Here we reconstructed, at high spatial resolution, the 3-dimensional structure of grass phytoliths using 3D X-ray microscopy. Simultaneously, we characterized the location of phytC using Nano-scale Secondary Ion Mass Spectrometry (NanoSIMS).

2. Material and methods

Grasses are among the main producers of phytoliths. The leaves of *Triticum durum* wheat (TD-F-L), were harvested in 2012 at the Genomics Research Centre in Fiorenzuola d'Arda (Italy). Hundreds grams were made available to us for phytC investigation. Phytoliths were extracted from 50g of dry leaves using a wet chemical protocol recently set up for geochemical analyses of phytC. The protocol was described in detail in Corbineau et al. (2013). The organic matter was oxidized with H_2SO_4, H_2O_2, HNO_3 and $KClO_3$, and potential remains on the phytolith surfaces were dissolved using KOH (pH@11). Absence of residual extraneous organic particles was checked using SEM-EDS (Corbineau et al., 2013). Dominant phytolith types were recognized according to Madella et al. (2005) using NL microscopy at 600X and 1000X magnifications. As expected, the Grass Short Cell group (GSC) and the Bulliform cell group dominated the assemblage. These groups, that form in all grass epidermis, also dominate

phytolith assemblages produced by grasslands and recovered from soils (e.g. Alexandre et al., 2011). Several NL microscopy and SEM pictures, illustrating the composition of the TD-F-L phytolith assemblage, were taken. For the purpose of morphological comparison, pictures of fossil GSC and bulliform phytoliths from available soil assemblages described in previous papers, were additionally taken.

The 3D structure of the GSC phytoliths was reconstructed by X-ray imaging at the micro-scale, using a 3D X-ray microscope Zeiss Ultra XRM L 200. A few phytoliths, randomly selected from the bulk sample, were deposited on the inner surface of a bevel-cut Kepton tube of 50µm of internal diameter. Five individual GSC phytoliths were recognized by optical microscopy at 200X magnification and their position located for 3D visualization. The principle of the 3D X-ray microscopy technique consists in focusing the X-ray beam on a rotating sample using optical lens; then transmitted x-rays are diffracted by a Fresnel zone plate on a scintillator in front of an optical device to produce a 200X magnified image of the phytolith captured by a CCD image sensor. Using a 1k x 1k detector, it leads to a voxel size of 63nm. X-ray beam path is continuously flushed with helium to minimize the absorption of X-rays by air, the sample and the optics excepted. While this technic has been widely used for 3D reconstruction of biological systems it has never been applied in high resolution mode to silica particles. Analyses of the phytoliths were proceeded at 150nm resolution for a 65µm field of view, in conventional absorption contrast imaging mode at 8keV (copper rotating anode; power set at 40kV and 30mA). Using this mode, the contrast was generated both from the different x-ray attenuation coefficients of the chemical elements composing the sample and from the density. Nine hundreds one x-ray projections were recorded between -90° and +90° at an angle step of 0.2° and an exposure time of 80s per view. After 20 hours of analysis, reconstruction of the phytolith volume was performed using XMReconstructor (Zeiss Xradia software). The resulting stack of 2D grayscale slices was then exported to Avizo Fire (FEI group) for further image processing.

NanoSIMS analyses were performed on cross sections of TD-F-L phytoliths embedded in epoxy resin. One mg of phytoliths was deposited on polytetrafluoroethylene (PTFE) filters (9mm i.d.) stuck on double face tape. Polypropylene (PP) tubes (10mm i.d. and 15 mm long) were placed on the tape, encircling the phytoliths. Epoxy resin (Araldite 100/hardener 16) was slip into the tubes up to 3 mm height and left to dry 3H at 40°C. Seven mm height of resin was added and left to dry 48H at 40°C. Those two steps prevented the resin to leak from the base of the tube. Embedded samples were taken off the tubes and polished with diamond paste up to 0.1 µm, until the PTFE filter was completely removed and cross sections of phytoliths were

visible in NL microscopy. Samples were sawn into 4mm thick blocks. Dozens of GSC phytoliths cross sections to be analyzed with the nanoSIMS were located by SEM. The nanoSIMS technique is based upon the sputtering of a few atomic layers from the surface of a sample induced by a primary ion bombardment. The primary ion impact triggers a cascade of atomic collision. Atoms and atomic clusters are ejected. During the ejection process, some atoms and clusters are spontaneously ionized. These secondary ions are characteristic of the composition of the analyzed area. They are separated according to their mass and an image of the intensity of the secondary ion beam is made for a selected mass (Cameca, 2014). Over the past few years, the NanoSIMS technique was increasingly used in geosciences, to investigate the elemental and isotopic composition of organic and inorganic materials (Herrmann et al., 2007; Hatton et al., 2012; Mueller et al., 2012; Carsten W. Mueller, 2013). The NanoSIMS technique was however scarcely used for measuring secondary ion emission from amorphous silica. One study showed nanoSIMS images of a thin section of a giant siliceous sponge spicule (several mm of diameter). A micrometric proteinaceous scaffold, which averaged 2% C dry weight, could be detected in the siliceous structure (Müller et al., 2010). The NanoSIMS technique was also used for identifying silicification sites in rice roots (Moore et al., 2011). Here, we analyzed the intensities of $[^{28}Si]^-$, $[^{16}O]^-$, $[^{24}C_2]^-$ and $[^{26}CN]^-$ ions produced by selected areas of the GSC phytoliths polished cross sections using a Cameca NanoSIMS 50. The section was coated with 25nm gold and introduced in the NanoSIMS. A $[Cs]^+$ primary ion probe with 16kV primary ion impact energy and a 8kV secondary ion extraction voltage was used. The best adjustment for obtaining secondary ion images of $[^{28}Si]^-$, $[^{16}O]^-$, $[^{12}C]^-$ and $[^{26}CN]^-$ was the following: the selected phytolith surfaces were first pre-sputtered with a defocused primary beam on a 60µmX60µm area during 3min. Then 256x256 pixel images were made using a 2.2 pA primary ion current (Primary Diaphragm Diameter = 300µm), a counting time of 10 ms per pixel for areas of 30µmX30µm. Analyses with longer counting time, larger primary diaphragm/higher primary beam intensity were also tested. Secondary ion images of $[^{28}Si]$, $[^{16}O]^-$, $[^{12}C]^-$ and $[^{26}CN]^-$ were processed using the ImageJ software (http://imagej.nih.gov/ij). Colors were assigned to different intensities of signal, increasing from black to red. Images of the $[^{26}CN]^-/[^{12}C]^-$ ratio were also created. Line-scans were drawn across the analyzed surfaces and ion intensity *vs* distance along the line were plotted.

For comparison with the NanoSIMS results, the C and N contents of the bulk TD-F-L phytolith sample were measured by chemiluminescence after combustion at 1350° (for C) and 1000°C

(for N). The C and N contents of the Epoxy resin were measured with an Elemental Analyzer (EA) after combustion at 1350°C.

3. Results

Three morphological categories of phytoliths, commonly found in grasses, constituted the bulk sample. SEM pictures of phytoliths placed on the aluminum mount illustrate these categories on figure 01. SEM pictures of cross sections of the same categories are shown on figure 02. For each category, the mode of silica deposition is specified below when it has been previously evidenced by MEB, MET, fluorescence microscopy or NanoSIMS images of plant cross sections (Sangster and Parry, 1969; Sowers and Thurston, 1979; Harrison, 1996; Currie and Perry, 2007; Law and Exley, 2011; Moore et al., 2011). The first phytolith category is constituted of thin fragments of multi-cellular silica sheets, several tenths of μm long and wide but less than a few micrometers thick (fig01a, 01b, 02a, 02b). These silica "skeletons"(Sangster and Parry, 1969; Law and Exley, 2011) were shown to result from the silicification of the middle lamella of the cells walls in grass epidermis and mesophyll, possibly as an early step of silicification (Laue et al., 2007; Law and Exley, 2012). Although abundant in plants (Piperno, 2006), the multi-cellular silica sheets are rapidly subjected to fragmentation and dissolution and are scarcely preserved in soils and sediments (Alexandre et al., 1996). The second phytolith category is constituted of stellate silica particles, of 10-15μm width (fig01c) that were shown to form in the intercellular spaces of the grass epidermis (Lins et al., 2002). This mode of silica precipitation was described as centripetal, starting as a narrow band lining the cavity, then infilling partially or completely the intercellular space (Sangster and Parry, 1981). The third category dominated the wheat phytolith assemblage. It is made of mono-cellular phytolith types of 10-50μm of length, width and thickness. Most of them are GSC phytoliths and belong to the Rondel (Fig01d, 01e) and Polylobate (fig01f) types. The formation of the mono-cellular phytolith type was also shown to be centripetal, starting in or against the cell walls and progressively infilling the lumen (e.g. Zhang et al., 2013). The processes that leads to complete silicification of the cells and to organic compounds occlusion are still unknown. Cellulose fibrils from the cell wall may regulate the silica formation (Laue et al., 2007).

SEM observation of cross sections of tenths of GSC phytoliths evidenced one or two internal cavities a few micrometers of diameter in the silica structure (fig02c, 02d, 02e). They were similar in shape and size as the low electron density round area visible on one of the TEM image

of phytoliths shown by Laue et al. (2007) (Fig. 2 B of Laue et al., 2007). However, SEM observation of the GSC phytoliths just placed on the aluminum mount did not evidence any holes on the phytolith surfaces. When observed in NL microscopy (fig03) the internal cavities were recognizable as opaque areas.

Two examples of reconstructed 3D X-ray microscopy volumes are presented in figures 04 and 05. The observed patterns were common to the five analyzed GSC particles. The siliceous structure appeared porous at the sub-micrometer scale (fig0 4A and 05A). Inside the structure, areas of a few micrometers of diameter, with significantly lower X-ray absorption than the surrounding, were observed (fig04A). 2D-planes of the reconstructed volumes evidenced that these heterogeneities were the cavities several micrometers wide previously identified on the cross sections by SEM. The cavities were interconnected (fig04B, 05B). Some particles showed cavities isolated from the phytolith surface by a few micrometers thick silica wall (fig04B). Other particles showed cavities connected to the phytolith surface by small holes of one-tenth micrometers of diameter only (fig05B). These cavities appeared filled with air (no X-ray absorption), although the high contrast in X-Ray absorbance between silica and air may have masked the presence of organic compounds.

The NanoSIMS results, common to the dozens of analyzed phytolith thin sections, are illustrated in Figures 06, 07 and 08. Adjustments were done to find the pre-sputtering duration (3 min), the primary ion beam intensity (L1=2kV), the primary diaphragm diameter (750µm) and the duration of analyses (11 min) appropriate for obtaining sufficient total ion current (TIC) and avoid charging effects (fig06A, 07A). When the primary ion beam intensity was increased to L1=4kV (fig08A), when the primary diaphragm diameter was decreased to 300µm (fig08B), or when a succession of analyses resulted in increasing the duration of sputtering (fig08C), a zone devoid of secondary ion signal appeared at the center of the silica surface. This was probably due to charging (Mueller et al., 2012) and/or to topographic heterogeneity (Winterholler et al., 2008). As silica was more resistant to polishing than the Epoxy, silica surfaces were often convex (fig08). The tests conducted here emphasized the importance of looking for the most efficient adjustment (i.e. avoiding charging and topographic effects) before performing NanoSIMS analyses on silica surfaces.

$[^{28}Si]^-$, $[^{16}O]^-$, $[^{12}C]^-$ and $[^{26}CN]^-$ images clearly individualized phytoliths from the Epoxy resin. The $[^{28}Si]^-$ and $[^{16}O]^-$ images and scan lines showed that phytoliths were made of a continuous silica structure (fig06, 07) sometimes interrupted by central micrometric areas devoid of silica (fig07). This is again in concordance with the central cavities identified in SEM and 3D-X-Ray

imaging. Carbon was present in the cavities and in the silica structure itself. However when values of $[^{12}C]^-$ intensity were similar in the cavities and in the Epoxy resin, they were 10 to 20 times lower in the silica structure than in the Epoxy resin (fig06, 07). N was also present in the silica structure and $[^{26}CN]^-$ intensity was 3 to 4 times lower in the silica structure than in the cavities or the Epoxy (fig06, 07). Interestingly, the ratio $[^{26}CN]^-/[^{12}C]^-$ ranged between 20 and 30 in the silica structure and between 5 and 10 in the cavities and the Epoxy. The silica structure was thus enriched in N by a 4 to 8 factor, relatively to the surrounding Epoxy. These features were reproducible from a particle to another. Bulk C and N contents in phytoliths, measured by chemiluminescence and EA (cf material and methods), were, for phytoliths 0.4 and 0.1% dry weight respectively, and for the Epoxy resin 68.8 and 2.8% dry weight respectively. The N/C ratio was 0.27 for the phytoliths and 0.04 for the Epoxy resin. The bulk phytolith sample was thus enriched in N relatively to the Epoxy resin by a factor 6.8, in agreement with N enrichments calculated from the NanoSIMS data. This consistency strengthened the accuracy of the $[^{12}C]^-$ and $[^{26}CN]^-$ relative intensities measured with the nanoSIMS. Finally, $[^{26}CN]^-/[^{12}C]^-$ NanoSIMS images clearly showed that organic compounds, with content in N significantly higher than in the resin, were continuously distributed (at the sub-micrometer scale) in the silica structure. To the contrary, cavities appeared filled with the Epoxy resin.

4. Discussion

4.1. PhytC locations in the silica structure of GSC phytoliths

SEM, 3D-X-Ray microscopy and NanoSIMS images showed that the silica structure of GSC phytoliths was homogeneous at the micrometric scale, and systematically contained central micrometric interconnected cavities. The fact that some particles contained cavities isolated from the outside suggests that the opening to the outside can be either original or result from dissolution posterior to the phytolith formation. Phytoliths often contain ‰ to % dry weight of aluminium (Al) (Bartoli and Wilding, 1980; Carnelli et al., 2004) co-precipitating with silica (Hodson and Sangster, 1993). As Al dissolves in strong acids and in strong bases, the phytolith chemical extraction procedure that included HNO_3 and H_2SO_4 steps, may have initiated phytolith surficial dissolution and opened the few micrometers thick silica wall between the cavities and the phytolith surface. The procedure also included a final alkaline step (KOH @ pH 11) that may also have increased the dissolution features on the silica surfaces. As phytoliths

were directly extracted from the plant, the surficial dissolution was revealed here at its beginning. It is expected to reach higher degree over time in natural environment where multiple dissolution factors come into play (Iler, 1979; Bartoli, 1983). Large dissolution features were indeed often observed on fossil phytoliths and were quantified to assess the degree of weathering of soil phytolith assemblages (Alexandre et al., 1999; Oleschko et al., 2004). To illustrate this point SEM and NL microscopy images of whole and cross sections of fossil mono-cellular phytoliths collected from soils are shown on Figure 09. The phytolith types are characteristic of grass epidermis (GSC types and Cuneiform bulliform types; Madella et al., 2005) (fig 09A, 09B) and wood parenchyma (Globular granulate type; Madella et al., 2005) (fig9C). The dissolution of silica has made central depressions of several micrometers wide. The particles appear empty inside, which is consistent with dissolution starting from the silica walls located between the cavities and the phytolith surfaces, then slightly opening, or increasing the opening of the cavities to the outside, then enlarging the cavities into dissolution depressions. Such dissolution depressions are not limited to GSC phytoliths. They were observed on many types of mono-cellular phytoliths from grasses and non-grasses extracted from soils and sediments as illustrated in Figure 9A5 (Acicular type), 9B2 and 9B3 (Globular granulate). This implies that the inner part of all these phytolith types was constituted of silica less dense than the outer part, either due to phytC occlusion or to a lack of dissolved Si available for precipitation during the phytolith formation.

Inside the internal cavities, no original organic compounds could be detected by NanoSIMS. If initially present, they may have been squeezed out and replaced by the Epoxy resin during the polishing step. To the contrary, the $[^{26}CN]^-/[^{12}C]^-$ images clearly evidenced the presence of organic compounds rich in N continuously distributed in the silica structure and clearly differentiated from the Epoxy resin. Absolute composition in $[^{26}CN]^-$ and $[^{12}C]^-$ were not calculated. This would have required to include in the analyzed section standard materials with known composition. However, the consistency of N enrichment of the organic compound in the silica structure (measured by NanoSIMS) with N enrichment of the bulk phytC (measured by chemiluminescences/EA), supports that the organic compound measured by NanoSIMS is phytC. Finally, although our data cannot conclude on the presence or not of any phytC in the internal cavities, they demonstrate that the phytC is, in a whole or in a part, continuously distributed in the silica structure.

4.2. Implications regarding phytC occlusion and phytC accessibility

Evidences of the continuous distribution of phytC in the silica structure, at the sub-micrometric scale, suggest that it was occluded since the early stage of silicification. SEM, environmental scanning electron microscope (ESEM) and TEM-EDX analyses showed that silica first precipitates in the inner cell wall, probably triggered by the presence of callose or lignin (Laue et al., 2007; Law and Exeley, 2012; Zhang et al., 2013). Silica nanospheres are then organized in a variety of structural motifs such as sheet-like, globular and fibrillar bundles that, from the cell wall, infill the cell lumen in a centripetal way (e.g. Kaufman et al., 1970; Robert et al., 1973; Sangster and Parry, 1981; Perry et al., 1984; Laue et al., 2007; Zhang et al., 2013), until most of the cell becomes silicified (Motomura, 2004; Laue et al., 2006). As previously noted, an organic template may participate to the silica formation (Harrison, 1996; Laue et al., 2007). This organic template, progressively trapped in the silica structure may constitute the phytC evidenced by NanoSIMS in the phytoliths. Its N/C value (0.27) is in the range of N/C values characteristic of amino acids. Amino acids may originate either from the cell itself or from the extra-cellular space. Different families of transporters have been identified for their import into plant cells (Tegeder, 2012). In the same time, amino acids entering the cell simultaneously to silica thanks to an invagination/vesicle formation mechanism previously evidenced (Neumann and De Figueiredo, 2002) may occur.

At the end of the cell silicification, residual cell organic compounds that were not already occluded may gather in a remaining space and delimitate the micrometric central cavities. This second pool of phytC should be rapidly oxidized when phytoliths start to dissolve after their deposition in litter, soil or sediment (fig.09). This suggests that this phytC pool participates in a limited extent to long term atmospheric CO_2 sequestration. These considerations rise the need to further estimate the respective contributions to C contents measured from bulk phytolith concentrates of (i) phytC in the silica structure, of (ii) phytC in the central cavities, and (iii) extraneous C that may remain on porous phytolith surfaces. This is a prerequisite for reliable assessments of the significance of phytC in atmospheric CO_2 sequestration.

4.3. Reassessment of NL microscopy observations

Several studies have speculated that opaque areas observed by NL microscopy in fossil phytoliths from soils and sediments were burnt organic remains indicative of past fire occurrence (Piperno, 1998; Kealhofer and Penny, 1998; Elbaum et al., 2003; Parr, 2006; Piperno, 2006). However, when observed by NL microscopy, the empty dissolution depressions evidenced by SEM on mono-cellular phytoliths from soils (fig09A) also appeared as opaque areas, especially when they were oriented downwards (fig09C). This is probably due to trapped

air in the dissolution depressions that caused optical artifact at the place where air met the mounting medium. This feature implies that opaque areas in fossil phytoliths should not be considered as unequivocal evidence of burnt organic compounds. Similarly, internal cavities may also appear as opaque spots due to the occurrence of trapped air, independently of the presence of organic compounds.

5. Conclusion

3D-XRay microscopy reconstructions of GSC phytoliths from harvested grasses, and SEM observations of their cross sections, showed that the silica structure contains micrometric internal cavities. These cavities were sometimes observed isolated from the outside. Their opening may be an original feature or may result from the silica dissolution during the chemical extraction procedure, mimicking the beginning of dissolution process that may happen in natural environments. The phytC that may originally occupy those cavities is thus susceptible to rapid oxidation. It was not detected by the nanoSIMS technique. To the contrary another pool of phytC, continuously distributed in and protected by the silica structure, was evidenced by nanoSIMS. Its N/C ratio (0.27) is in agreement with the presence of amino acids. These findings constitute a basis to further characterize the origin, occlusion process, nature and accessibility of phytC, necessary for assessing its significance in the global C cycle.

Aknowledgements

The authors gratefully acknowledge the support from LABEX OT-Med (France) (2013-2014 grant to AA), from the U.S. National Science Foundation (DEB-1144888 to GMS) and from the “Investissements d’Avenir” French Government program of the French National Research Agency that founded the French X-ray CT platform Nano-ID (ANR-10-EQPX-39-01). NanoSIMS analyses were conducted at the Plateforme NanoSIMS, OSUR, Université de Rennes 1, France. We express special thanks to Franz Badeck and Luigi Cattivelli (CRA - Genomic Research Centre, Fiorenzuola d'Arda, Italy) for providing the wheat sample.

References

Alexandre, A., Meunier, J. D., Mariotti, A., and Soubies, F.: Late Holocene phytolith and carbon isotope record from a latosol at Salitre, south-central Brazil, Quaternary Res., 51, 187–194, 1999.

Alexandre, A., Bouvet, M., and Abbadie, L.: The role of savannas in the terrestrial Si cycle: a case-study from Lamto, Ivory Coast, Global Planet. Change, 78, 162–169, 2011.

Alexandre, A., Crespin, J., Sylvestre, F., Sonzogni, C., and Hilbert, D. W.: The oxygen isotopic composition of phytolith assemblages from tropical rainforest soil tops (Queensland, Australia): validation of a new paleoenvironmental tool, Clim. Past, 8, 307–324, doi:10.5194/cp- 8-307-2012, 2012.

Blecker, S.W., McCulley, R. L., Chadwick, O. A., and Kelly, E. F.: Biologic cycling of silica across a grassland bioclimosequence, Global Biogeochem. Cy., 20, doi:10.1029/2006gb002690, 2006.

Carnelli, A. L., Theurillat, J. P., and Madella, A.: Phytolith types and type-frequencies in subalpine-alpine plant species of the European Alps, Rev. Palaeobot. Palyno., 129, 39–65, 2004.

Carter, J. A.: Atmospheric carbon isotope signatures in phytolith-occluded carbon, Quatern. Int., 193, 20–29, 2009.

Corbineau, R., Reyerson, P. E., Alexandre, A., and Santos, G. M.: Towards producing pure phytolith concentrates from plants that are suitable for carbon isotopic analysis, Rev. Palaeobot. Palyno., 197, 179–185, 2013.

Cornelis, J.-T., Delvaux, B., Georg, R. B., Lucas, Y., Ranger, J., and Opfergelt, S.: Tracing the origin of dissolved silicon transferred from various soil-plant systems towards rivers: a review, Biogeosciences, 8, 89–112, doi:10.5194/bg-8-89-2011, 2011.

Currie, H. A. and Perry, C. C.: Silica in plants: biological, biochemical and chemical studies, Ann. Bot., 100, 1383–1389, 2007.

Elbaum, R., Weiner, S., Albert, R. M., and Elbaum, M.: Detection of burning of plant materials in the archaeological record by changes in the refractive indices of siliceous phytoliths, J. Archaeol. Sci., 30, 217–226, 2003.

Elbaum, R., Melamed-Bessudo, C., Tuross, N., Levy, A. A., and Weiner, S.: New methods to isolate organic materials from silicified phytoliths reveal fragmented glycoproteins but no DNA, Quatern. Int., 193, 11–19, 2009.

Gao, Y., Cheng, Z., Ling, W., and Huang, J.: Arbuscular mycorrhizal fungal hyphae contribute to the uptake of polycyclic aromatic hydrocarbons by plant roots, Bioresource Technol., 101, 6895–6901, 2010.

Harrison, C. C.: Evidence for intramineral macromolecules containing protein from plant silicas, Phytochemistry, 41, 37–42, 1996.

Hatton, P.-J., Remusat, L., Zeller, B., and Derrien, D.: A multi-scale approach to determine accurate elemental and isotopic ratios by nano-scale secondary ion mass spectrometry imaging, Rapid Commun. Mass Sp., 26, 1363–1371, 2012.

20 Herrmann, A. M., Clode, P. L., Fletcher, I. R., Nunan, N., Stockdale, E. A., O'Donnell, A. G., and Murphy, D. V.: A novel method for the study of the biophysical interface in soils using nano-scale secondary ion mass spectrometry, Rapid Commun. Mass Sp., 21, 29–34, 2007.

Hodson, M. J. and Sangster, A. G.: The interaction between silicon and aluminium in *Sorghum bicolor* (L.) Moench: growth analysis and X-ray microanalysis, Ann. Bot., 72, 389–400, 1993.

Huang, Z., Li, Y., Jiang, P., Chang, S. X., Song, Z., Liu, J., and Zhou, G.: Long-term intensive management increased carbon occluded in phytolith (PhytOC) in bamboo forest soils, Sci. Reports, 4, doi:10.1029/2006gb002690 , 2014.

Instruments-for-research: SIMS, available at: http://www.cameca.com/instruments-forresearch/ sims.aspx, 2014.

Kealhofer, L. and Penny, D.: A combined pollen and phytolith record for fourteen thousand years of vegetation change in northeastern Thailand, Rev. Palaeobot. Palyno., 103, 83–93, 1998. 14714

Kelly, E. F., Amundson, R. G., Marino, B. D., and Deniro, M. J.: Stable isotope ratios of carbon in phytoliths as a quantitative method of monitoring vegetation and climate change, Quat. Res., 35, 222–233, 1991.

Laue, M., Hause, G., Dietrich, D., and Wielage, B.: Ultrastructure and microanalysis of silica bodies in *Dactylis glomerata* L., Microchim. Acta, 156, 103–107, 2006.

Law, C. and Exley, C.: New insight into silica deposition in horsetail (*Equisetum arvense*), BMC Plant Biol., 11, doi:10.1038/srep03602, 2011.

Li, B., Song, Z., Li, Z., Wang, H., Gui, R., and Song, R.: Phylogenetic variation of phytolith carbon sequestration in bamboos, Sci. Reports, 4, doi:10.1038/srep04710, 2014.

Lins, U., Barros, C. F., da Cunha, M., and Miguens, F. C.: Structure, morphology, and composition of silicon biocomposites in the palm tree *Syagrus coronata* (Mart.) Becc., Protoplasma, 220, 89–96, 2002.

Madella, M., Alexandre, A., Ball, T., and Grp, I.W.: International code for phytolith nomenclature 1.0, Ann. Bot., 96, 253–260, 2005.

McInerney, F. A., Strömberg, C. A. E., andWhite, J.W. C.: The Neogene transition from C3 to C4 grasslands in North America: stable carbon isotope ratios of fossil phytoliths, Paleobiology, 37, 23–49, 2011.

McMichael, C. H., Bush, M. B., Silman, M. R., Piperno, D. R., Raczka, M., Lobato, L. C., Zimmerman, M., Hagen, S., and Palace, M.: Historical fire and bamboo dynamics in western Amazonia, J. Biogeogr., doi:10.1111/jbi.12002, 2012.

Miller, L. A., Smith, S. Y., Sheldon, N. D., and Strömberg, C. A. E.: Eocene vegetation and ecosystem fluctuations inferred from a high-resolution phytolith record, Geol. Soc. Am. Bull., B30548.1, 2012.

Motomura, H.: Silica deposition in relation to ageing of leaf tissues in *Sasa veitchii* (Carriere) Rehder (Poaceae: Bambusoideae), Ann. Bot., 93, 235–248, 2004.

Mueller, C. W., Kölbl, A., Hoeschen, C., Hillion, F., Heister, K., Herrmann, A. M., and Kögel-Knabner, I.: Submicron scale imaging of soil organic matter dynamics using NanoSIMS – from single particles to intact aggregates, Org. Geochem., 42, 1476–1488, 2012.

Müller, W.E., Wang, X., Cui, F.Z., Jochum, K.P., Tremel, W., Bill, J., Schröder, H.C., Natalio, F., Schlossmacher, U., and Wiens, M. (2009). Sponge spicules as blueprints for the biofabrication of inorganic-organic composites and biomaterials. Applied Microbiology and Biotechnology *83*, 397–413.

Müller, W. E. G., Wang, X., Sinha, B., Wiens, M., Schröder, H.-C., and Jochum, K. P.: NanoSIMS: insights into the organization of the proteinaceous scaffold within Hexactinellid sponge spicules, Chembiochem, 11, 1077–1082, 2010.

Neumann, D. and De Figueiredo, C.: A novel mechanism of silicon uptake, Protoplasma, 220, 59–67, 2002.

Oleschko, K., Parrot, J.-F., Ronquillo, G., Shoba, S., Stoops, G., and Marcelino, V.: Weathering: toward a fractal quantifying, Math. Geol., 36, 607–627, 2004.

Parr, J. F.: Effect of fire on phytolith coloration, Geoarchaeology, 21, 171–185, 2006.

Parr, J. F. and Sullivan, L. A.: Soil carbon sequestration in phytoliths, Soil Biol. Biochem., 37, 117–124, 2005.

Parr, J. F. and Sullivan, L. A.: Comparison of two methods for the isolation of phytolith occluded carbon from plant material, Plant Soil, 374, 45–53, 2014.

Parr, J., Sullivan, L., Chen, B., Ye, G., and Zheng, W.: Carbon bio-sequestration within the phytoliths of economic bamboo species, Glob. Change Biol., 16, 2661–2667, 2010.

Paungfoo-Lonhienne, C., Lonhienne, T. G. A., Rentsch, D., Robinson, N., Christie, M., Webb, R. I., Gamage, H. K., Carroll, B. J., Schenk, P. M., and Schmidt, S.: Plants can use protein as a nitrogen source without assistance from other organisms, P. Natl. Acad. Sci. USA, 105, 4524–4529, 2008.

Piperno, D. R.: Phytoliths: a Comprehensive Guide for Archaeologists and Paleoecologists, Rowman Altamira, 2006.

Piperno, D. R. and Becker, P.: Vegetational history of a site in the central Amazon Basin derived from phytolith and charcoal records from natural soils, Quaternary Res., 45, 202–209, 1996.

Piperno, D. R. and Stothert, K. E.: Phytolith evidence for early Holocene Cucurbita domestication in southwest Ecuador, Science, 299, 1054–1057, 2003.

Pironon, J., Meunier, J. D., Alexandre, A., Mathieu, R., Mansuy, L., Grosjean, A., and Jarde, E.: Individual characterization of phytoliths: experimental approach and consequences on paleoenvironment understanding, edited by: A. A. Balkema, Lisse, 2001.

Prychid, C. J., Rudall, P. J., and Gregory, M.: Systematics and biology of silica bodies in monocotyledons, Bot. Rev., 69, 377–440, 2003.

Sangster, A. G. and Parry, D. W.: Some factors in relation to bulliform cell silicification in the grass leaf, Ann. Bot., 33, 315–323, 1969.

Santos, G. M., Alexandre, A., Coe, H. H. G., Reyerson, P. E., Southon, J. R., and De Carvalho, C. N.: The phytolith C-14 puzzle: a tale of background determinations and accuracy tests, Radiocarbon, 52, 113–128, 2010.

Santos, G. M., Alexandre, A., Southon, J. R., Treseder, K. K., Corbineau, R., and Reyerson, P. E.: Possible source of ancient carbon in phytolith concentrates from harvested grasses, Biogeosciences, 9, 1873–1884, doi:10.5194/bg-9-1873-2012, 2012.

Smith, F. A. and Anderson, K. B.: Characterization of organic compounds in phytoliths: improving the resolving power of phytolith delta C-13 as a tool for paleoecological reconstruction of C3 and C4 grasses, in: Phytoliths – Applications in Earth Science and Human History, edited by: Meunier, J. D., and Colin, CRC Press, 317–327, 2001.

Smith, F. A. and 5 White, J. W. C.: Modern calibration of phytolith carbon isotope signatures for C3/C4 paleograssland reconstruction, Palaeogeogr. Palaeocl., 207, 277–304, 2004.

Song, Z., Wang, H., Strong, P. J., Li, Z., and Jiang, P.: Plant impact on the coupled terrestrial biogeochemical cycles of silicon and carbon: implications for biogeochemical carbon sequestration, Earth-Sci. Rev., 115, doi:10.1016/j.earscirev.2012.09.006, 2012.

Song, Z., Wang, H., Strong, P. J., and Guo, F.: Phytolith carbon sequestration in China's croplands, Eur. J. Agron., 53, 10–15, 2014.

Sowers, A. E. and Thurston, E. L.: Ultrastructural evidence for uptake of silicon-containing silicic acid analogs by *Urtica pilulifera* and incorporation into cell wall silica, Protoplasma, 101, 11–22, 1979.

Strömberg, C. A. E., Dunn, R. E., Madden, R. H., Kohn, M. J., and Carlini, A. A.: Decoupling the spread of grasslands from the evolution of grazer-type herbivores in South America, Nat. Commun., 4, 1478, doi:10.1038/ncomms2508, 2013.

Tegeder, M.: Transporters for amino acids in plant cells: some functions and many unknowns, Curr. Opin. Plant Biol., 15, 315–321, 2012.

Warren, C. R.: Post-uptake metabolism affects quantification of amino acid uptake, New Phytol., 193, 522–531, 2012.

Watling, K. M., Parr, J. F., Rintoul, L., Brown, C. L., and Sullivan, L. A.: Raman, infrared and XPS study of bamboo phytoliths after chemical digestion, Spectrochim. Acta A, 80, 106–111, 2011.

Webb, E. A. and Longstaffe, F. J.: Limitations on the climatic and ecological signals provided by the delta C-13 values of phytoliths from a C4 North American prairie grass, Geochim. Cosmochim. Ac., 74, 3041–3050, 2010.

Whiteside, M. D., Treseder, K. K., and Atsatt, P. R.: The brighter side of soils: quantum dots track organic nitrogen through fungi and plants, Ecology, 90, 100–108, 2009.

Whiteside, M. D., Garcia, M. O., and Treseder, K. K.: Amino acid uptake in arbuscular mycorrhizal plants, PLoS ONE, 7, e47643, doi:10.1371/journal.pone.0047643, 2012.

Winterholler, B., Hoppe, P., Foley, S., and Andreae, M. O.: Sulfur isotope ratio measurements of individual sulfate particles by NanoSIMS, Int. J. Mass Spectrom., 272, 63–77, 2008.

Zhang, C., Wang, L., Zhang, W., and Zhang, F.: Do lignification and silicification of the cell wall precede silicon deposition in the silica cell of the rice (*Oryza sativa* L.) leaf epidermis?, Plant Soil, 372, 137–149, 2013.

Zuo, X., Lu, H., and Gu, Z.: Distribution of soil phytolith-occluded carbon in the Chinese Loess Plateau and its implications for silica–carbon cycles, Plant Soil, 374, 223–232, 2014.

Figures captions

Figure 1. SEM images of TD-F-L wheat phytolith assemblage, deposited on aluminum mount. Three categories are illustrated: 1) silica sheets (a,b), 2) stellate type from intercellular space (c) and 3) GSC phytoliths including Rondel type (d,e) and Polylobate type (f).

Figure 2. SEM images of the thin section of the TD-F-L wheat phytolith types including silica sheets (a,b), and GSC phytoliths of the Rondel type (c,d,e). GSC types show micrometric internal cavities (IC).

Figure 3. NL microscopy images of grass short cell (GSC) phytolith types from the wheat TD-F-L sample showing opaque areas (O).

Figure 4: 3D X-ray microscopy of a GSC phytolith from wheat (TD-F-L): **A**: four view of the reconstructed volumes; internal cavities (IC) are distinguishable. **B**: 2D x-ray slices superimposed on the phytolith volume rendering showing from front to back the internal cavity (IC). No connection to the surfaces was evidenced. The blue area corresponds to the thresholding of the phytolith grayscale values.

Figure 5: 3D X-ray microscopy of a GSC phytolith from wheat (TD-F-L): **A**: reconstructed volume. **B**: 2D X-ray images from back to front of the phytolith showing the internal cavity (IC) and its connection to the surfaces forming holes (H). The blue area corresponds to the thresholding of the phytolith grayscale values.

Figure 6. NanoSIMS images and intensities of a first typical GSC phytolith (Rondel type) from TD-F-L (wheat) embedded in Epoxy resin (polished section). Pre-sputtering: L1=2kV defocused (60X60mm) $[Cs]^+$ primary beam, during 3min **A**: $[^{28}Si]^-$, $[^{16}O]^-$, $[^{12}C_2]^-$, $[^{12}C\ ^{14}N]^-$ and $[^{12}C\ ^{14}N]^-/\ [^{12}C_2]^-$ images obtained with a $[Cs]^+$ primary beam with L1=2kV, D1-1 primary diaphragm (750µm), during 11min; **B**: Secondary ion intensities along line scans (red line in Fig. 6A).

Figure 7. NanoSIMS images and intensities of a second typical GSC phytolith (Rondel type) from TD-F-L (wheat) embedded in Epoxy resin (polished section). Pre-sputtering: L1=2kV defocused (60X60mm) $[Cs]^+$ primary beam, during 3min **A**: $[^{28}Si]^-$, $[^{16}O]^-$, $[^{12}C_2]^-$, $[^{12}C\ ^{14}N]^-$ and $[^{12}C\ ^{14}N]^-/\ [^{12}C_2]^-$ images obtained with a $[Cs]^+$ primary beam with L1=2kV, D1-1 primary diaphragm (750µm), during 11min; **B**: $[^{28}Si]^-$ image obtained with a $[Cs]^+$ primary beam increased with L1=4kV , D1-1 primary diaphragm , during 11min; **C**: Secondary ion intensities along line scans (red line in Fig. 5A).

Figure 8. SEM images of the polished section showing convex silica surfaces (Si) in the Epoxy resin (r). Associated NanoSIMS $[^{28}Si]^-$ images showing central areas devoid of secondary ion signal. **A**: $[Cs]^+$ primary beam with L1=4kV, D 1-1 primary diaphragm (750mm), 11min; **B**: $[Cs]^+$ primary beam with L1=2kV, D 1-2 primary diaphragm (300μm), 11min; **C**: $[Cs]^+$ primary beam with L1=2kV, D1-1 primary diaphragm (750μm), 3min analyses for successively 1,2 and 3.

Figure 9. NL microscopy and SEM images of dissolution depressions (DD) affecting fossil phytoliths from soils. **A**: Grass epidermis monocellular phytoliths (Cuneiform Bulliform types and Acicular type) from Mascareignite (MSG 70, La Réunion, France) (Crespin et al., 2008); NL microscopy phytolith surface (1, 2), SEM phytolith volume (3) and polished section (4, 5). **B**: Grass epidermis monocellular phytoliths from a ferrugineous soil (Salitre, Brazil) (Alexandre et al., 1999); NL microscopy phytolith **C**: Phytoliths from palms and trees from a ferallitic soil (Dimonika, RDA) (Alexandre et al., 1997); SEM Globular granulate type volumes (1, 2) and polished section (3). **D**: Opaque areas observed in NL microscopy on bulliform cell phytoliths from MSG 70 (1,2) and Salitre (3,4). Scale bars: 10μm.

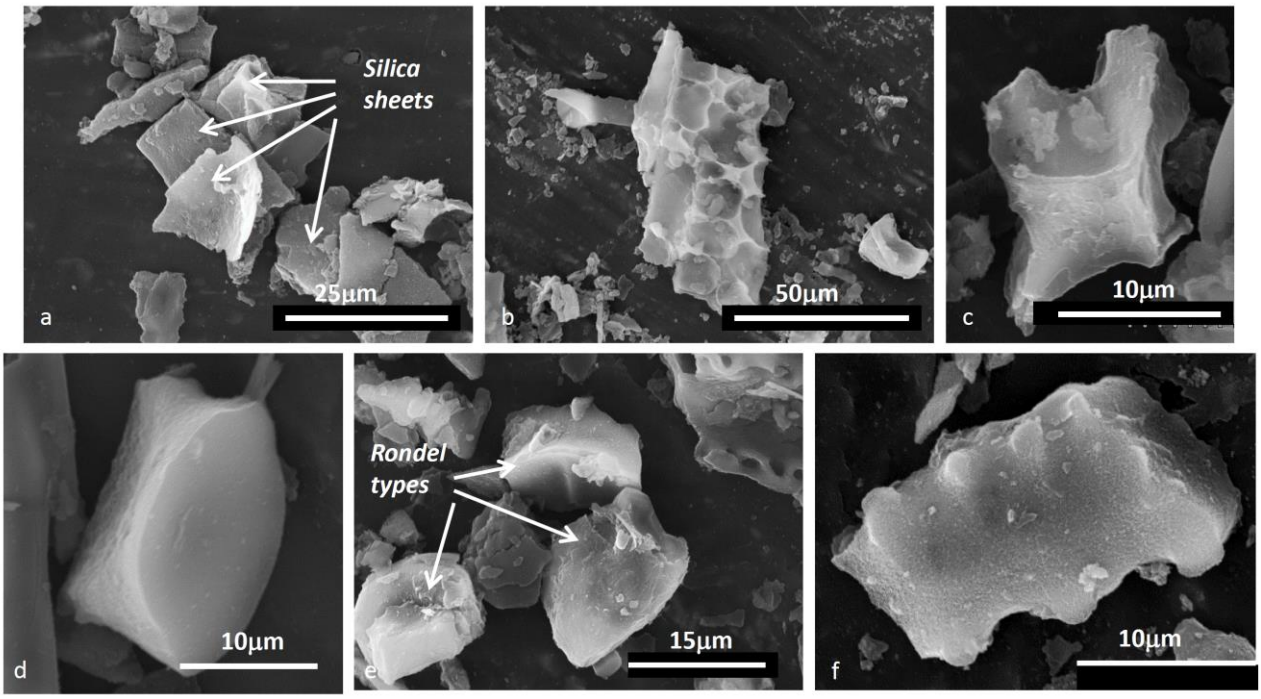
Silica
sheets
25µm
a
50µm
b
10µm
c
10µm
d
Rondel
types
15µm
e
10µm
f

Figure 1.

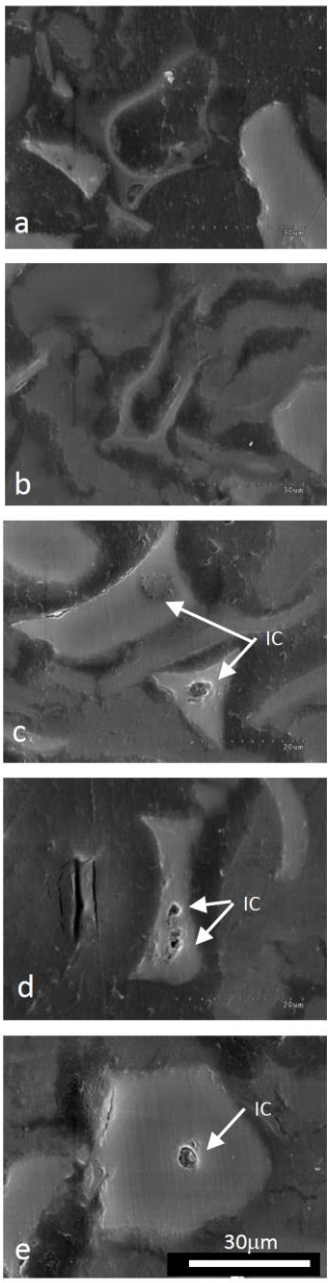

Figure 2.

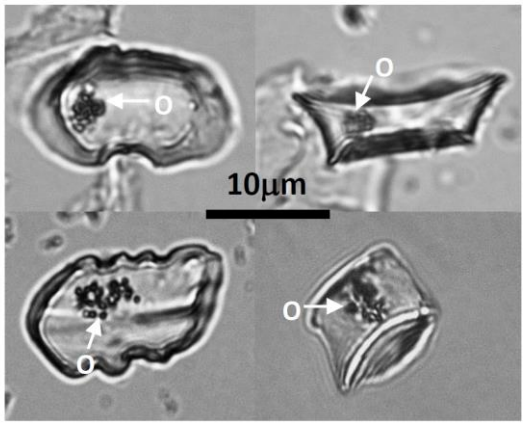

Figure 3.

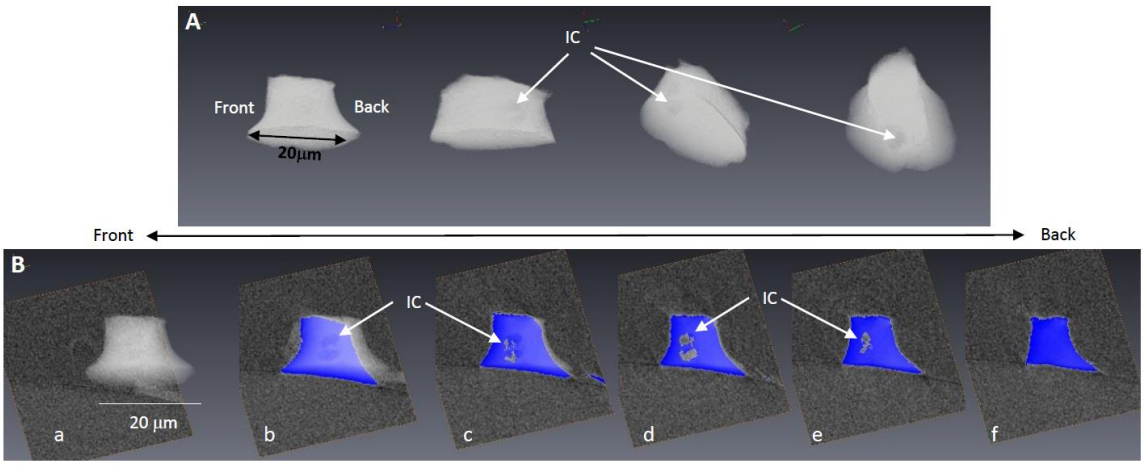

Figure 4

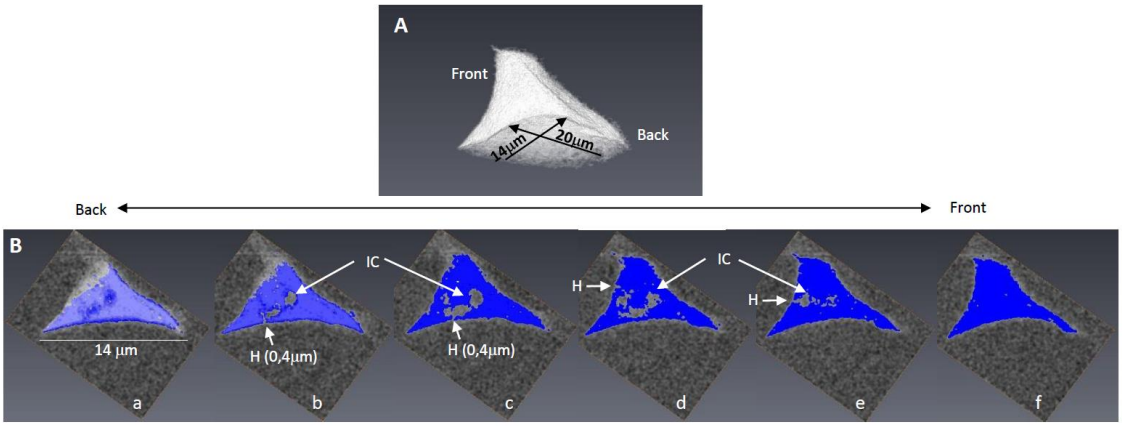
A
Front
Back
14µm
20µm
Back
Front
B
14 µm
IC
H (0,4µm)
IC
H (0,4µm)
H
IC
H
a
b
c
d
e
f

Figure 5

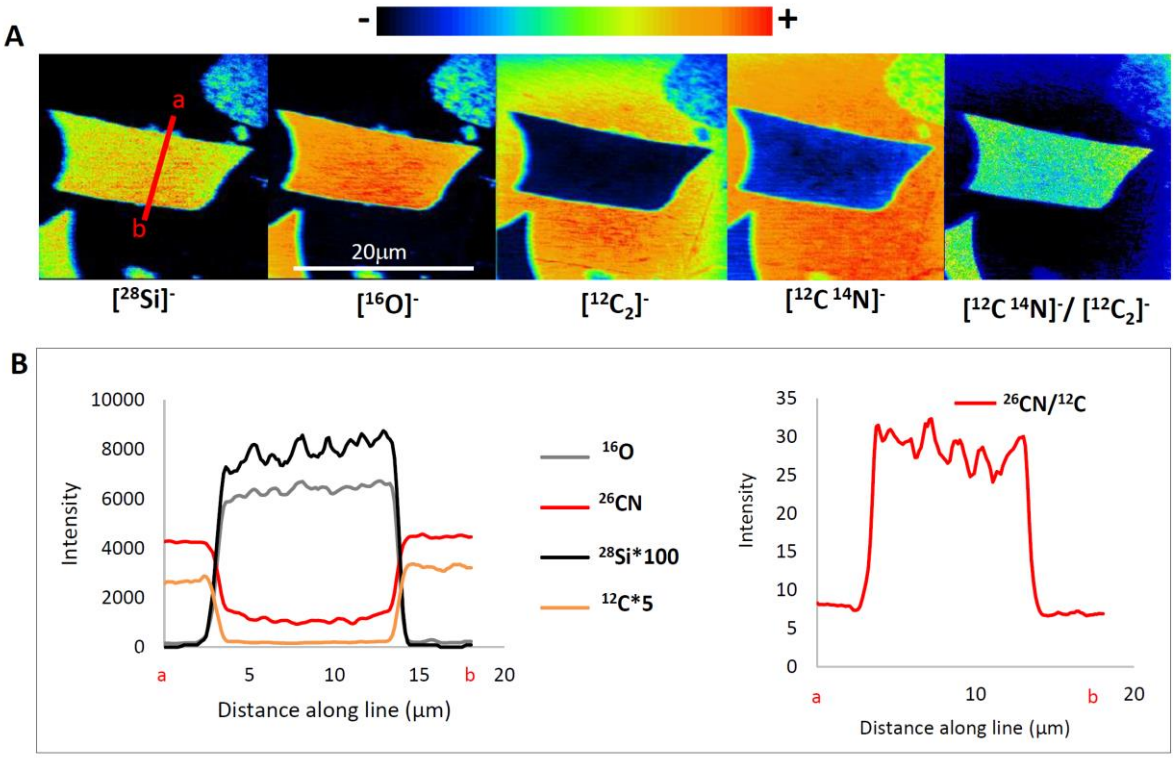
A
-
+
a
b
20µm
[28Si]-
[16O]-
[12C2]-
[12C 14N]-
[12C 14N]-/ [12C2]-
B
Intensity
10000
8000
6000
4000
2000
0
a
5
10
15
b
20
Distance along line (µm)
16O
26CN
28Si*100
12C*5
Intensity
35
30
25
20
15
10
5
0
a
10
b
20
Distance along line (µm)
26CN/12C

Figure 6.

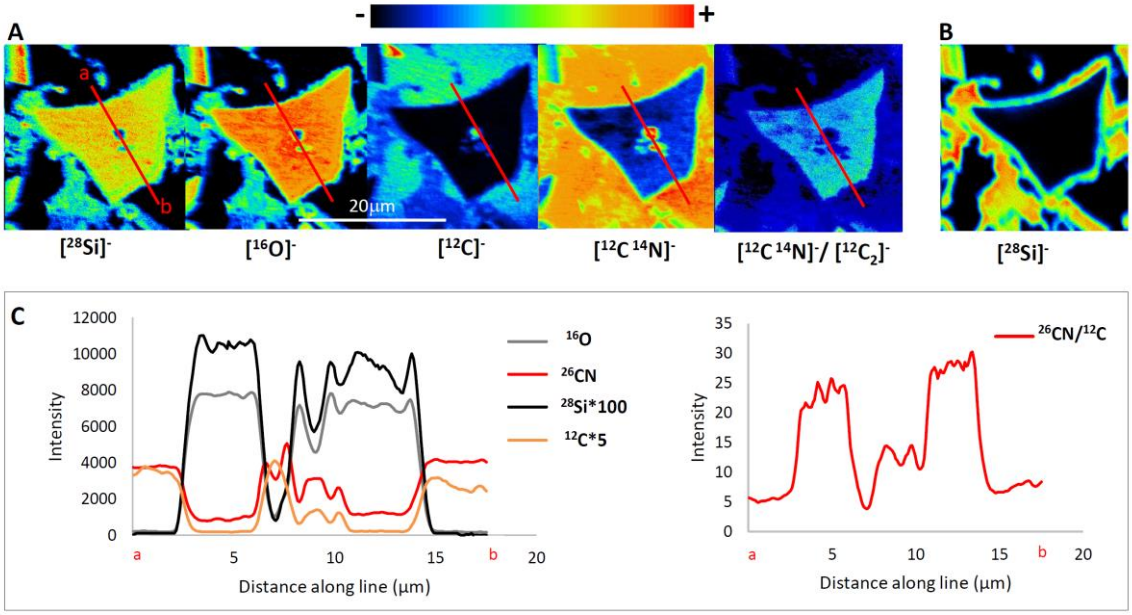
A
B
-
+
a
b
20µm
[28Si]-
[16O]-
[12C]-
[12C 14N]-
[12C 14N]-/ [12C2]-
[28Si]-
C
Intensity
Distance along line (µm)
16O
26CN
28Si*100
12C*5
26CN/12C

Figure 7.

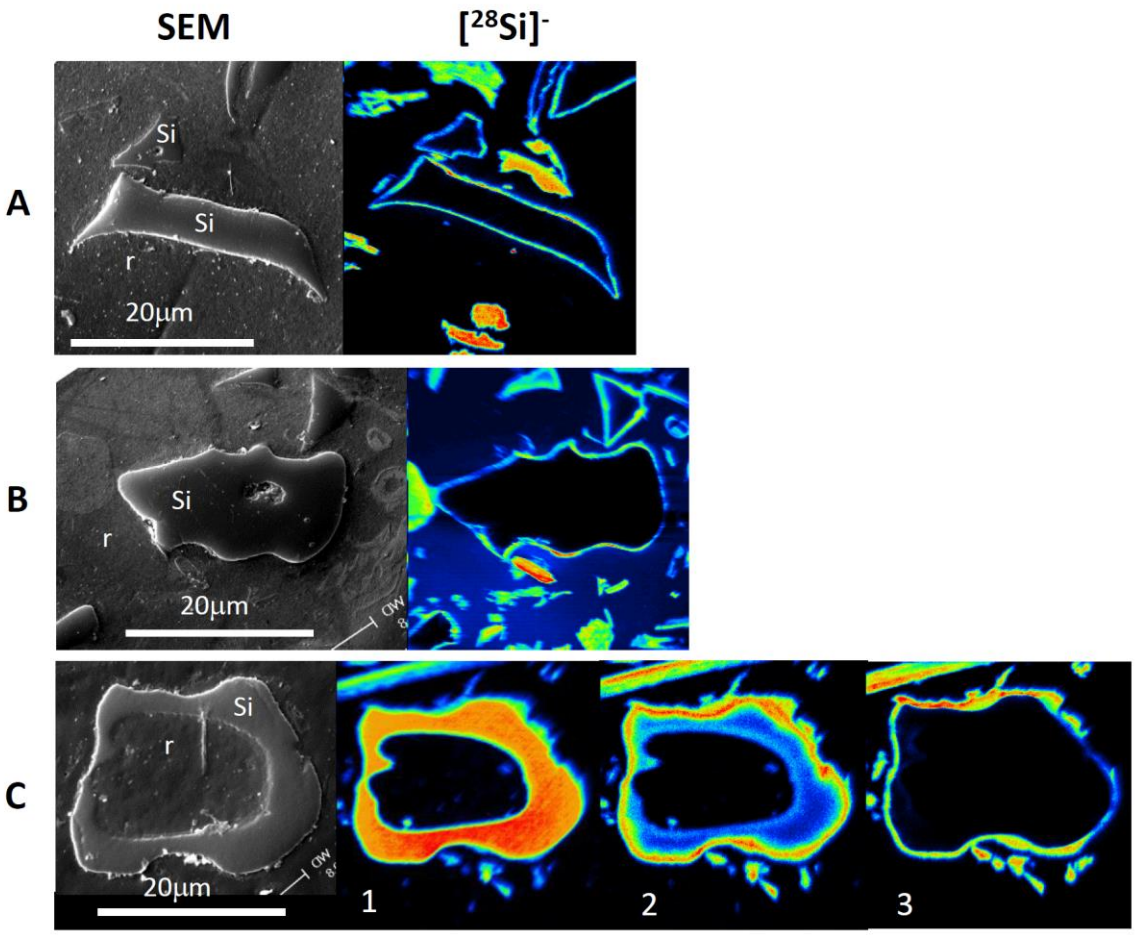

Figure 8.

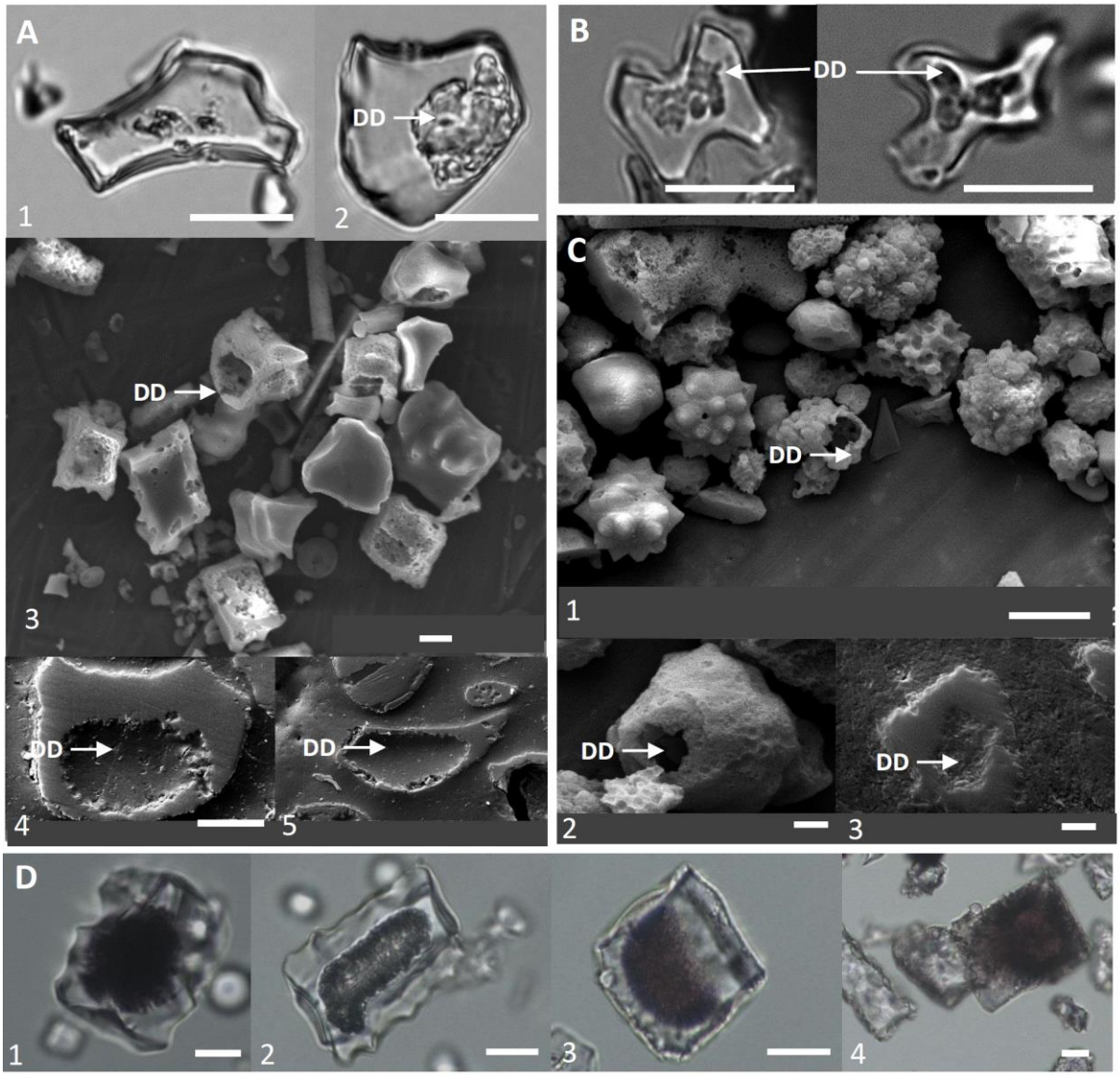

Figure 9.